Chem. Res. Chin. Univ., 2017, 33(4), 638—642 doi: 10.1007/s40242-017-7026-9

One-pot Hydrothermal Synthesis of Novel $NiCoO_2$/Reduced Graphene Oxide Composites for Supercapacitors

WANG Hongzhi, SHI Xin, SHI Yulei, ZHANG Weiguo* and YAO Suwei
Department of Applied Chemistry, School of Chemical Engineering and Technology, Tianjin University, Tianjin 300350, P. R. China

Abstract Novel $NiCoO_2$/rGO composites with a structure of $NiCoO_2$ nanoparticles anchored on layers of reduced graphene oxide(rGO) were synthesized *via* a simple one-pot hydrothermal method and were used as faradaic electrodes for supercapacitors. The microstructures of $NiCoO_2$/rGO composites were characterized by means of field emission scanning electron microscopy(FESEM), transmission electron microscopy(TEM), X-ray diffraction(XRD) and thermogravimetric analysis(TGA). When acting as faradaic electrodes for supercapacitors, $NiCoO_2$/rGO composites exhibited a specific capacity of 288 C/g at the current density of 2 A/g and maintained 139.98 C/g at 20 A/g. High capacity retention ratios up to 88% could be achieved after 1000 cycles at a current density of 2 A/g. The outstanding cycling stability was primarily attributed to the combination of mixed transition metal oxides and rGO, which not only maintains a high electrical conductivity for the overall electrode but also prevents the aggregation and volume expansion of electrochemical materials during the cycling processes.

Keywords $NiCoO_2$; rGO; Composite; Faradaic electrode; Supercapacitor

1 Introduction

Due to the advancing wheels of the global economy, the need for efficient and environmentally friendly methods of energy conversion and storage becomes increasingly urgent[1—5]. Supercapacitors, which bridge the gap between traditional capacitors and rechargeable batteries, have drawn considerable attention, especially in the field of electric vehicles, due to their high power density, rapid charging/recharging rate and long cycle life[6—9]. As is well-known, electrode material is the most important component of supercapacitors, which affects supercapacitors' performance to a large extent. Many researchers are aiming at producing new substances and constructs to achieve better properties for supercapacitors[3,10—14]. Currently, there is a confusion regarding the definition of "pseudocapacitive materials" and "battery-type materials." According to the mechanism of storing an electrical charge, materials that exhibit faradaic behavior during the charge-discharge process are more likely to be defined as a type of battery-type material than as a pseudocapacitive material[15]. Therefore, the materials' electrochemical properties can be better evaluated by specific capacity(C/g) than specific capacitance(F/g).

Transition metal oxides are a class of promising battery-type materials. First, these metals possess superb capabilities to store charge, similar to carbon materials. Additionally, there are rich faradaic redox reactions provided by multiple valence states in transition metal oxides. Therefore, researchers have focused on inexpensive, abundant and environmentally friendly transition metal elements, such as Co, Mn and Ni[16—18]. It has been determined that the mixed transition metal oxides can perform better in electrical conductivity and capacity than single-component[18—20]. There are various reports regarding the synthesis and properties of $NiCo_2O_4$ in the field of energy storage, while few studies focused on $NiCoO_2$[21—24]. Due to the electrically insulating nature, low working potential and poor cycle stability of $NiCoO_2$, the practical applications of $NiCoO_2$ are restricted. To address this problem, it would be expedient to combine a capacitor-type material with $NiCoO_2$ to achieve synergistic effects between the two types of materials. As a novel two-dimensional single-atom-thick carbon material with a honeycomb lattice structure, graphene has attracted huge research interest in both academy and industry[25,26]. Its unique structural features provide excellent mechanical, thermal, and optical properties. In particular, its great theoretical specific surface area and high electronic conductivity make graphene a promising material for high-performance supercapacitors[27—31]. However, there are still several considerable barriers preventing graphene's effective application in supercapacitors. The foremost obstacles are serious aggregation and restacking of graphene, which not only decrease its actual specific surface area but also hinder the rapid transport of electrolyte ions[32,33].

In our study, we described a facile one-pot hydrothermal strategy for the fabrication of $NiCoO_2$/rGO composites. Due to positive synergistic effects, the composites maintained a high electrical conductivity, a distinct volume change cushion, and an effective prevention of rGO's agglomeration or restacking during the charge-discharge process. Moreover, for improved

*Corresponding author. E-mail: zwg@tju.edu.cn
Received January 16, 2017; accepted February 13, 2017.
Supported by the Natural Science Foundation of Tianjin City, China(No.11JCYBJC01900).

accuracy, we employed metric specific capacity(C/g) instead of specific capacitance(F/g) to evaluate the electrochemical performance of this battery-type composite.

2 Experimental

2.1 Synthesis of $NiCoO_2$/rGO Composites

Graphite oxide was prepared by a modified Hummers method as reported earlier[34]. Typically, 144 mg of sodium dodecyl sulfate(SDS) was dissolved into 40 mL of 0.5 mg/mL GO aqueous dispersion, with ultrasonication for 30 min. Next, 20 mL of mixed solution, which contained 0.1 mmol of $Ni(NO_3)_2$ and $Co(NO_3)_2$(Co:Ni =1:1, molar ratio), was slowly added to the solution. After ultrasonication for another 1 h, $NH_3 \cdot H_2O$ was slowly added to the solution until the pH reached 11. Next, the mixture was stirred with a magnetic stirrer for another 12 h. After that, 0.75 mmol of urea was added to the solution and the solution was stirred for 30 min. Subsequently, the resulting suspension was transferred into a 100 mL Teflon-lined autoclave, and heated to 180 °C for 6 h. The precipitate was rinsed with deionized water and ethanol several times. Afterwards, the as-prepared product was subjected to calcination in nitrogen atmosphere at 300 °C for 2 h. Similarly, pure rGO was obtained by the same procedure with GO and solvent alone. Pure $NiCoO_2$ was synthesized in the absence of GO.

2.2 Characterization Methods

X-Ray diffraction(XRD) patterns were collected on a Bruker D-8 instrument(Cu $K\alpha$ radiation, λ=0.154056 nm). Thermogravimetric analysis(TGA) was performed on a TG8120 in air atmosphere. The morphologies and microstructures of the as-prepared samples were characterized by means of field emission scanning electron microscopy(FESEM, Hitachi S4800, Japan), transmission electron microscopy(TEM, JEM 3100F JEOL, Japan), X-ray photoelectron spectroscopy (XPS, PHI 1600 photoelectron spectrometer) and Raman spectroscopy(DXR Raman Microscope).

2.3 Electrochemical Measurement

The electrochemical measurements were performed in a 6 mol/L KOH aqueous solution as the electrolyte, and using a three-electrode setup: Ni foam coated with electroactive materials as the working electrodes, platinum foil and saturated calomel electrode(SCE) as the counter and reference electrodes, respectively. Electrochemical studies including cyclic voltammetry(CV), galvanostatic charge-discharge(GCD) and electrochemical impedance spectroscopy(EIS) were carried out on a CHI 660B electrochemical workstation at room temperature.

3 Results and Discussion

3.1 Morphology and Structure Characterization

XRD patterns of $NiCoO_2$, rGO and $NiCoO_2$/rGO composites are shown in Fig.1(A) patterns *a*—*c*. As shown in Fig.1(A) pattern *a*, all diffraction peaks of $NiCoO_2$ are perfectly in accordance with the standard data of cubic $NiCoO_2$(JCPDS No. 10-0188), indicating the pure quality of the as-prepared sample. Meanwhile, the strong and narrow diffraction peaks show that the material possesses high crystallinity. In Fig.1(A) pattern *b*, the broad diffraction peak of rGO appearing at approximately 25° corresponds to the (002) plane of graphene. As shown in Fig.1(A) pattern *c*, the diffraction peaks of $NiCoO_2$/rGO composites are similar to that of $NiCoO_2$. The additional diffraction peak attributes of rGO indicate that the $NiCoO_2$/rGO composites are well synthesized.

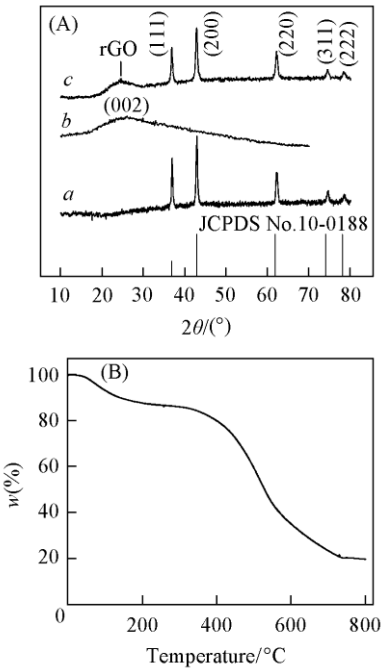

Fig.1 XRD patterns(A) of $NiCoO_2$(*a*), rGO(*b*) and $NiCoO_2$/rGO composites(*c*) and TG curve of $NiCoO_2$/rGO composites in air atmosphere(B)

The composition of $NiCoO_2$/rGO composites can be further investigated by TGA, which was performed up to 800 °C in air with a heating rate of 10 °C/min. As shown in Fig.1(B), there is an initial mass loss of approximately 10% below 200 °C, which is associated with the deintercalation of surface-absorbed water. Subsequently, $NiCoO_2$/rGO composites display a dramatic mass loss from approximately 400 °C to 700 °C, and this fully 64% of mass loss should be attributed to the removal of carbon sketch by burning rGO, while the remainder is $NiCoO_2$, which has a better thermal property[35]. Therefore, it can be deduced that the mass percentage of $NiCoO_2$ nanoparticle in the composite is 19.9%, while that of rGO is 80.1%.

The microstructures and morphologies of $NiCoO_2$/rGO composites were investigated by means of FESEM and TEM. As shown in Fig.2(A), the $NiCoO_2$ nanoparticles with particle sizes ranging from 250 nm to 420 nm are anchored on the layers of rGO. Moreover, owing to the hydrothermal conditions, the rGO sheets curled up to form a flower-like structure, and the $NiCoO_2$ nanoparticles anchored on these “petals,” which can be confirmed by the TEM image in Fig.2(B). The structure is beneficial to improving the electrical conductivity of the

overall electrode and effectively preventing the restacking of rGO sheets in the charge-discharge process. From the TEM image in Fig.2(C) we can see that rGO sheets are coated on the outer surface of $NiCoO_2$ nanoparticle, which is in accordance with the SEM image. The magnification of the black part in Fig.2(C) is shown as the HRTEM image in Fig.2(D). The lattice spacing of 0.24, 0.21 and 0.13 nm all match well with the (111), (200) and (311) planes of the $NiCoO_2$ phase, respectively.

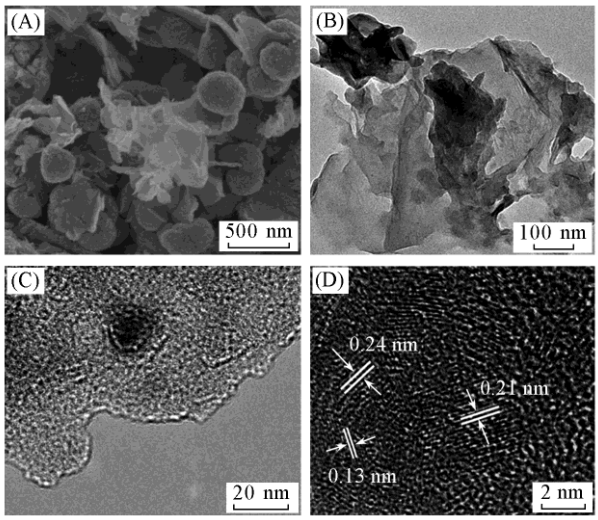

Fig.2 FESEM image(A), TEM image(B) and high resolution TEM images(C, D) of $NiCoO_2$/rGO composites

In addition, XPS was employed to analyze the surface information and chemical state of elements in $NiCoO_2$/rGO composites[Fig.3(A)—(E)]. As shown in Fig.3(A), the survey spectrum of $NiCoO_2$/rGO composites mainly confirms the presence of carbon, oxygen, cobalt and nickel species. In Fig.3(B), the major peak of the Co_{2p} XPS spectrum can be assigned to the $Co_{2p_{3/2}}$(approximately 782.4 eV). In Fig.3(C), the major peak of the Ni_{2p} XPS spectra can be assigned to the $Ni_{2p_{3/2}}$(approximately 857.0 eV). The Co_{2p} and Ni_{2p} XPS spectra show that both the cobalt and nickel elements in the composites exist in the bivalent form, which is in accordance with results from the XRD. Moreover, the peak located at 284.6 eV is assigned to the characteristic peak of C_{1s}, and a detailed deconvolution of the C_{1s} spectrum is shown in Fig.3(D). It is noteworthy that there are two types of carbon bonds, including C—C at 284.6 eV and C—O at 286.4 eV. The detailed deconvolution of the O_{1s} spectrum is shown in Fig.3(E), in which the peak located at 531.2 eV can be assigned to the bonds of Co—O and Ni—O, while the peak located at 531.2 eV can be assigned to the bonds of C—OH and C—OOH. The presence of these residual oxygen-containing groups can be attributed to the partial reduction of GO during the hydrothermal process. However, these hydrophilic groups can act as anchoring sites to enable $NiCoO_2$ to interact tightly with rGO. Moreover, these groups can enhance the wettability of the electrode, which brings a further positive effect on the compatibility between the electrode and the electrolyte. The Raman spectra of pure GO and $NiCoO_2$/rGO composites are shown in Fig.3(F). It can be clearly observed that there are three intense peaks at 1350, 1590 and 2700 cm^{-1} in both samples, corresponding to D, G and 2D bands, respectively. In general, the peak intensity ratio between the D and G bands(I_D/I_G) can be used to roughly estimate the disorder degree and average size of the domains of the graphitic materials. Compared to GO, the I_D/I_G ratio of the $NiCoO_2$/rGO composites increased from 0.96 to 1.06, owing to the decrease in size of the sp^2 graphitic domains during the thermal process, as well as the presence of some unrepaired defects[36]. The more disordered carbon structure in $NiCoO_2$/rGO composites compared to GO may be attributed to the introduction of $NiCoO_2$.

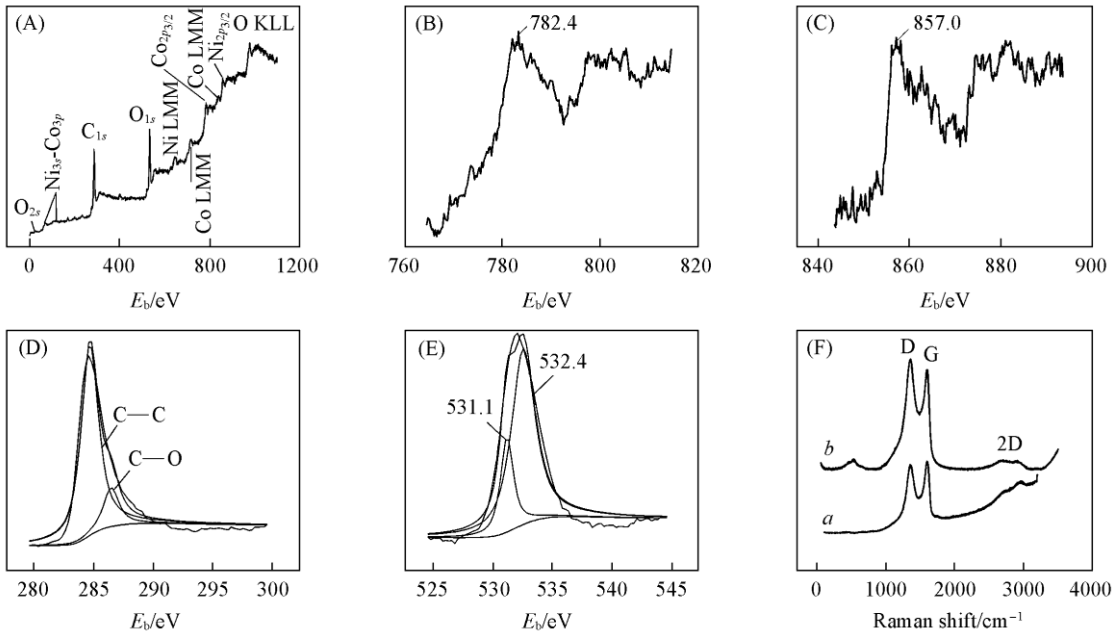

Fig.3 XPS spectra of $NiCoO_2$/rGO composites[(A)—(E)] and Raman spectra(F) of GO(*a*) and $NiCoO_2$/rGO composites(*b*)

(A) Survey spectrum; (B) Co_{2p} spectrum; (C) Ni_{2p} spectrum; (D) C_{1s} spectrum; (E) O_{1s} spectrum.

3.2 Electrochemical Measurement

To explore the electrochemical behavior of the $NiCoO_2$/rGO electrode, CV and GCD tests were conducted. From Fig.4(A), CV curves cycled at 20 mV/s on the $NiCoO_2$/rGO electrode show a pair of redox peaks, which differs from the CV curves of rGO displaying a rectangular shape. Fig.4(B) shows the CV curves on the $NiCoO_2$/rGO composite electrodes at scan rates of from 5 mV/s to 100 mV/s. The strong pairs of peaks in the CV curves indicate that the capacitive behavior is mainly attributed to faradaic redox reaction. The faradaic behavior is consistent with a battery-type electrode, coming from the following redox reaction:

$$NiCoO_2+2OH^- \rightleftharpoons NiOOH+CoOOH+2e \quad (1)$$

In Fig.4(C), the obvious plateau regions in the GCD curve of $NiCoO_2$/rGO electrode demonstrate faradaic behaviors caused by redox reactions, which is in accordance with the CV results. In addition, GCD curves on $NiCoO_2$/rGO composites at various current densities ranging from 2 A/g to 20 A/g were also employed[Fig.4(D)]. The specific capacities[C_s(C/g)] of $NiCoO_2$/rGO composites can be calculated from the following equation:

$$C_s = \frac{I\Delta t}{m} \quad (2)$$

where I(A) is the constant discharge current applied, Δt(s) is the discharge time, and m(g) is the mass of the active material. According to Eq.(2), the specific capacities of the $NiCoO_2$/rGO composites are calculated at current densities of 2, 3, 4, 5, 10 and 20 A/g, respectively[Fig.4(E)]. The specific capacity of the $NiCoO_2$/rGO composites is 288 C/g at the current density of 2 A/g and maintains 139.98 C/g at 20 A/g.

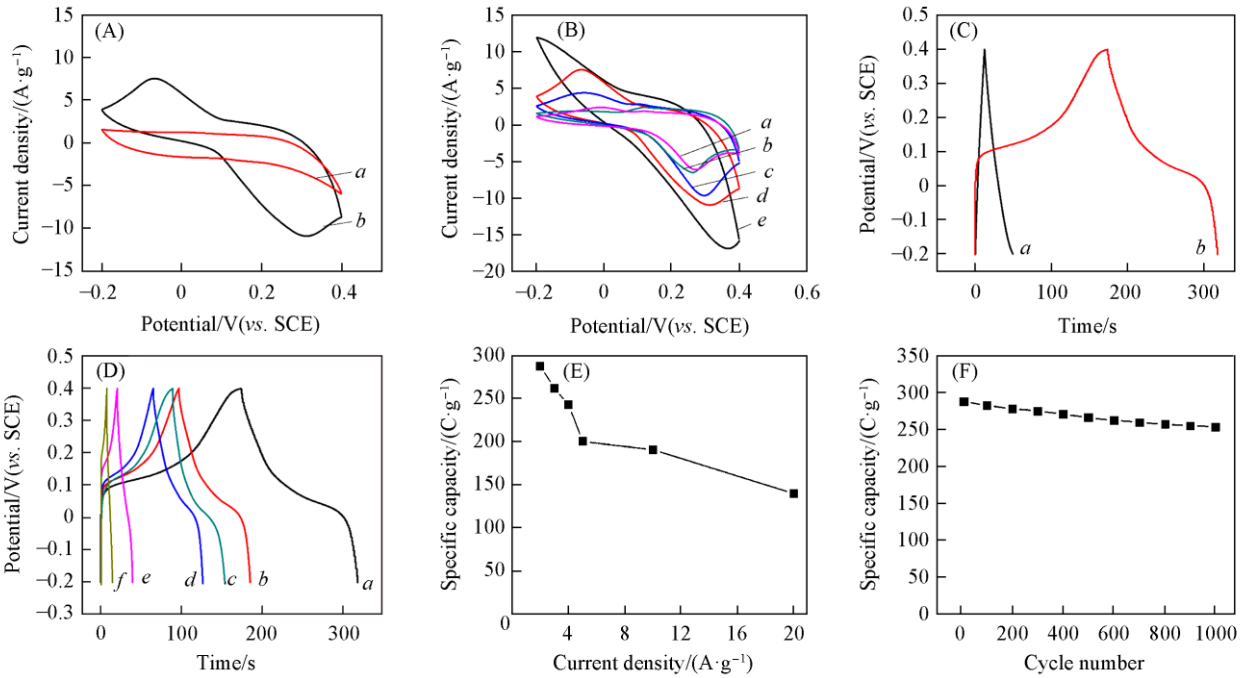

Fig.4 CV curves(A) of rGO(*a*) and $NiCoO_2$/rGO composites(*b*) at a scan rate of 20 mV/s, CV curves(B) of $NiCoO_2$/rGO composites at various scan rates, GCD plots(C) of rGO(*a*) and $NiCoO_2$/rGO composites(*b*) at a current density of 2 A/g, GCD plots(D) of $NiCoO_2$/rGO composites at various current densities, specific capacities(E) of $NiCoO_2$/rGO composites at various current densities and cycling performance(F) of $NiCoO_2$/rGO composites at a current density of 2 A/g

(B) Scan rate/(mV·s^{-1}): *a*. 5; *b*. 10; *c*. 20; *d*. 50; *e*. 100; (D) current density/(A·g^{-1}): *a*. 2; *b*. 3; *c*. 4; *d*. 5; *e*. 10; *f*. 20.

The long-term cycling performance of the $NiCoO_2$/rGO electrode at a current density of 2 A/g is shown in Fig.4(F). Notably, the $NiCoO_2$/rGO composites show a cycle performance with 88% capacity retention after 1000 cycles of charging and discharging. This outstanding cycling stability is closely related to the combination of $NiCoO_2$ and rGO. The unique hybrid architecture can maintain a high electrical conductivity for the overall electrode, which promotes a fast faradaic charging and discharging process on the composites. Moreover, the aggregation and volume expansion/collapse of electrochemical materials can be effectively prevented during the cycling processes by virtue of the hybrid structure.

EIS measurement is also a significant parameter for examining the fundamental behavior of $NiCoO_2$/rGO composites. The typical Nyquist plots for rGO and $NiCoO_2$/rGO electrodes are displayed in Fig.5. This pattern of plots can be fitted to an equivalent circuit[Fig.5(B)], where R_s, R_{ct}, Z_w, C_d, C_f are denoted as electrode series resistance, charge transfer resistance, Warburg impedance, electric double layer capacitance and faradaic capacitance, respectively[37]. From Fig.5(A), we can see that $NiCoO_2$/rGO displays a slightly bigger R_s value(1.227 Ω) than that of rGO(0.788 Ω), indicating that the outstanding electronic conductivity of rGO is maintained in $NiCoO_2$/rGO composites. Moreover, the charge transfer resistance(R_{ct}) of $NiCoO_2$/rGO composites is estimated to be 4.778 Ω, which is bigger than that of pure rGO. This can be attributed to the following facts: a portion of the charges in $NiCoO_2$/rGO composites is used to transfer between the rGO

sheets, and the remainder is used to participate in the faradaic redox reaction. In addition, the $NiCoO_2$/rGO composite electrode exhibits a line that is more vertical than rGO in the low frequency region, indicating the fast ion diffusion in the electrolyte, and the adsorption onto the electrode surface.

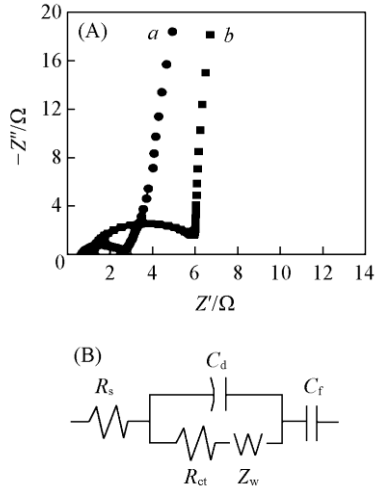

Fig.5 EIS spectra(A) of rGO(*a*) and $NiCoO_2$/rGO(*b*) electrodes in the frequency range from 100 kHz to 0.01 Hz and the electrical equivalent circuit(B) used for fitting the impedance spectra of $NiCoO_2$/rGO

4 Conclusions

We demonstrated a facile synthesis of novel $NiCoO_2$/rGO composites with the structure of $NiCoO_2$ nanoparticles anchored on layers of rGO through a one-pot hydrothermal route, and we investigated their electrochemical performance as a faradaic electrode for supercapacitors. It has been observed that the $NiCoO_2$/rGO composites exhibit an improved capacitive performance, which can be attributed to the combination of mixed transition metal oxides and rGO. Owing to the synergistic effects between the two kinds of materials, there is efficient charge transport and electrolyte diffusion during the charge-discharge process. Moreover, the aggregation and volume expansion/contraction of electrochemical materials can be effectively prevented. The composites achieve a specific capacity of 288 C/g at the current density of 2 A/g and maintain 139.98 C/g at 20 A/g. High capacity retention ratios up to 88% can be achieved after 1000 cycles at a current density of 2 A/g. These features make the $NiCoO_2$/rGO composite a suitable and promising electrode material for efficient supercapacitors. Moreover, this one-pot hydrothermal method can be easily generalized to other syntheses of mixed transition metals and carbon materials for supercapacitors.

References

[1] Conway B. E., *J. Electrochem. Soc*., **1991**, *138*, 1539
[2] Miller J. R., Simon P., *Science Magazine*, **2008**, *321*, 651
[3] Liu C., Li F., Ma L. P., Cheng H. M., *Adv. Mater.*, **2010**, *22*, E28
[4] Simon P., Gogotsi Y., Dunn B., *Science*, **2014**, *343*, 1210
[5] Wang H., Feng H., Li J., *Small,* **2014**, *10*, 2165
[6] Wang Y., Song Y., Xia Y., *Chem. Soc. Rev.*, **2016**, *45*, 5925
[7] Liu L., Niu Z., Chen J., *Chem. Soc. Rev.*, **2016**, *45*, 4340
[8] Yu Z., Tetard L., Zhai L., Thomas J., *Energy Environ. Sci*., **2015**, *8*, 702
[9] Yan J., Wang Q., Wei T., Fan Z., *Advanced Energy Materials*, **2014**, *4*, 157
[10] Simon P., Gogotsi Y., *Nat Mater.*, **2008**, *7*, 845
[11] Guo Y. G., Hu J. S., Wan L. J., *Adv. Mater.*, **2008**, *20*, 2878
[12] Frackowiak E., *Phy. Chem. Chem. Phy.*, **2007**, *9*, 1774
[13] Wang Q., Wen Z. H., Li J. H., *Advanced Functional Materials,* **2006**, *16*, 2141
[14] Liu H., He P., Li Z., Liu Y., Li J., *Electrochimica Acta,* **2006**, *51*, 1925
[15] Brousse T., Bélanger D., Long J. W., *J. Electrochem. Soc.*, **2015**, *162*, A5185
[16] Pramanik A., Maiti S., Sreemany M., Mahanty S., *Electrochimica Acta*, **2016**, *213*, 672
[17] Zhou Q., Wang X., Liu Y., He Y., Gao Y., Liu J., *J. Electrochem. Soc.*, **2014**, *161*, A1922
[18] Zhang G., Lou X. W. D., *Sci. Rep.*, **2013**, *3*, 1470
[19] Wu H. B., Pang H., Lou X. W. D., *Energy Environ. Sci.*, **2013**, *6*, 3619
[20] Yuan C., Li J., Hou L., Zhang X., Shen L., Lou X. W. D., *Adv. Fun. Mater.*, **2012**, *22*, 4592
[21] Zhang G., Lou X. W. D., *Adv. Mater.*, **2013**, *25*, 976
[22] Huang L., Chen D., Ding Y., Feng S., Wang Z. L., Liu M., *Nano Letters*, **2013**, *13*, 3135
[23] Lei Y., Li J., Wang Y., Gu L., Chang Y., Yuan H., Xiao D., *ACS Applied Materials & Interfaces*, **2014**, *6*, 1773
[24] Zhang X., Xu Y., *Materials Letters*, **2017**, *189*, 78
[25] Stoller M. D., Park S., Zhu Y., An J., Ruoff R. S., *Nano Lett.*, **2008**, *8*, 3498
[26] Geim A. K., Novoselov K. S., *Nat. Mater.*, **2007**, *6*, 183
[27] Yi H., Wang H., Jing Y., Peng T., Wang Y., Guo J., He Q., Guo Z., Wang X., *J. Mater. Chem. A*, **2015**, *3*, 19545
[28] Yan H., Bai J., Wang B., Yu L., Zhao L., Wang J., Liu Q., Liu J., Li Z., *Electrochimica Acta*, **2015**, *154*, 9
[29] Min S., Zhao C., Zhang Z., Wang K., Chen G., Qian X., Guo Z., *RSC Adv.*, **2015**, *5*, 62571
[30] Min S., Zhao C., Zhang Z., Chen G., Qian X., Guo Z., *J. Mater. Chem. A*, **2015**, *3*, 3641
[31] Xia J., Chen F., Li J., Tao N., *Nature Nanotechnology,* **2009**, *4*, 505
[32] Stoller M. D., Park S., Zhu Y., An J., Ruoff R. S., *Nano Letters*, **2008**, *8*, 3498
[33] Wang Y., Shi Z., Huang Y., Ma Y., Wang C., Chen M., Chen Y., *J. Phy. Chem. C*, **2009**, *113*, 13103
[34] Marcano D. C., Kosynkin D. V., Berlin J. M., Sinitskii A., Sun Z., Slesarev A., Alemany L. B., Lu W., Tour J. M., *ACS Nano*, **2010**, *4*, 4806
[35] Xu X., Zhou H., Ding S., Li J., Li B., Yu D., *J. Power Sources*, **2014**, *267*, 641
[36] Tuinstra F., Koenig J. L., *J. Chem. Phy.*, **1970**, *53*, 1126
[37] Di Fabio A., Giorgi A., Mastragostino M., Soavi F., *J. Electrochem. Soc.*, **2001**, *148*, A845